Delft University of Technology

Mechanistic DNA damage simulations in Geant4-DNA Part 2

Electron and proton damage in a bacterial cell

Lampe, Nathanael; Karamitros, Mathieu; Breton, Vincent; Brown, Jeremy M.C.; Sakata, Dousatsu; Sarramia, David; Incerti, Sébastien

Important note
To cite this publication, please use the final published version (if applicable).
Please check the document version above.

Original paper

Mechanistic DNA damage simulations in Geant4-DNA Part 2: Electron and proton damage in a bacterial cell

Nathanael Lampe[a,b], Mathieu Karamitros[b], Vincent Breton[a], Jeremy M.C. Brown[c],
Dousatsu Sakata[b], David Sarramia[a], Sébastien Incerti[b,*]

[a] Université Clermont Auvergne, CNRS/IN2P3, LPC, F-63000 Clermont-Ferrand, France
[b] Université de Bordeaux, CNRS/IN2P3, CENBG, F-33175 Gradignan, France
[c] Radiation Science and Technology, Delft University of Technology, Mekelweg 15, Delft 26295B, The Netherlands

ARTICLE INFO

ABSTRACT

We extended a generic Geant4 application for mechanistic DNA damage simulations to an *Escherichia coli* cell geometry, finding electron damage yields and proton damage yields largely in line with experimental results. Depending on the simulation of radical scavenging, electrons double strand breaks (DSBs) yields range from 0.004 to 0.010 DSB Gy^{-1} Mbp^{-1}, while protons have yields ranging from 0.004 DSB Gy^{-1} Mbp^{-1} at low LETs and with strict assumptions concerning scavenging, up to 0.020 DSB Gy^{-1} Mbp^{-1} at high LETs and when scavenging is weakest. Mechanistic DNA damage simulations can provide important limits on the extent to which physical processes can impact biology in low background experiments. We demonstrate the utility of these studies for low dose radiation biology calculating that in *E. coli*, the median rate at which the radiation background induces double strand breaks is 2.8×10^{-8} DSB day^{-1}, significantly less than the mutation rate per generation measured in *E. coli*, which is on the order of 10^{-3}.

1. Introduction

When modelling DNA damage mechanistically, simplistic geometries can be used to explore damage models [1], but realistic cellular geometries need to be built when considering cellular damage, as large scale geometrical order can impact the yield of single and double strand breaks (SSBs and DSBs). Recent work has focused on the implementation of such geometries for human cells, notably in the KURBUC [2,3] and PARTRAC [4,5] platforms, as well as a recent simulation chain based around combining several simulations in Geant4 10.1 [6–8], hereafter referred to as M16. By modelling physical track structures, radiation chemistry, and both direct and indirect DNA damage in a realistic geometry, these simulation platforms allow early biological damage from ionising radiation to be better understood [9]. Having already quantified how frequently background radiation interacts with cells [10] from measurements of the cosmic and terrestrial background spectrum, including gamma radiation, electrons, muons and neutrons [11], in this work, we investigate SSB and DSB yields in a realistic bacterial genome, corresponding to *Escherichia coli* as part of a larger project that is trying to estimate the mutational impact of background radiation.

Mechanistic DNA damage simulations have often been used to

better understand clinical contexts as a natural extension of micro- and nano-dosimetrically accurate track structure codes [12–14]. They can produce DSB yields in line with those observed experimentally, and can be coupled to DNA repair models that allow cellular damage from radiation to be understood from the 'bottom-up', and thus serve an important role in bridging the gap between physical processes and more 'top-down' models of radiation damage such as the Local Effect Model [15,16] and the Microsimetric Kinetic Model [17]. Our interest in mechanistic DNA damage simulations comes from how they can be used to place limits on responses to radiation at background and below background doses [18]. Biological experiments in underground laboratories and radiation affected environments have revealed biological behaviours that run contradictory to many expectations of radiation response. These include reduced growth rates when cells are grown below the radiation background [19,20] and changes in anti-oxidant levels when birds live in highly radioactive areas [21]. However modelling based on the physics of radiation suggests that radiation interactions alone cannot explain all the changes observed in these studies [22,23]. In this sense, physical modelling of low radiation backgrounds can place limits on what biological responses physics alone can be responsible for. This enables us to implicate other biological processes in the radiation response of cells at low doses, including

intercellular communication, regulatory changes, and possibly epigenetics. For this reason, we have chosen to model a bacterial cell as an example case for our method, as it complements our existing studies. The application used here though is generic, and could be one day configured to simulate other cell types.

In this work, we model the impact of electrons and protons on bacterial DNA, and draw comparisons to a variety of existing data. Based on our simulations of the impact of electron damage, we estimate the rate of double strand breaks in *E. coli* coming from the radiation background. We present first our method, explaining separately the physical, chemical and geometrical aspects of our simulation, before presenting our results. We explore the implications of our electron and proton damage measurements first, before tying our results into a prediction about the impact of the radiation background on DNA.

2. Method

Our method is built around a single Geant4 (v10.3) application that can simulate physical and chemical radiation damage in arbitrary DNA geometries, using Geant4-DNA physics and chemistry models [24–26]. A full description of the application is already available [27] and beyond the scope of this work, though to summarise, the application builds DNA geometries out of simply generated DNA definition files, which define a series of repeating DNA units, such as turned and straight DNA sequences, that can be used to build a continuous chain. These are defined as placement volumes internally in Geant4. A separate file is required to specify where these placement volumes are to be placed inside the Geant4 simulation. The application includes a command driven interface for defining regions of interest as well as commands for varying most simulation parameters.

The DNA chain itself is modelled as a sequence of spherical deoxyribose (sugar) and phosphate molecules, with the guanine, adenine, cytosine and thymine bases being modelled as ellipses. The spheres and ellipses were cut along one axis, to avoid overlaps in the geometry. Each placement volume is associated with an octree, so that from any given position, nearby molecules can be located, a requirement for both chemical simulations, and our model for attributing physical damage.

2.1. Physics

Physics was simulated using the Geant4-DNA Option 4 physics list. The models in this list are built around the Emfietzoglou dielectric model for water [28] used in the default list for electrons above 10 keV, and a refinement of the dielectric approach below 10 keV which redistributes the imaginary part of the dielectric function, ensuring more physically motivated behavior close to the binding energies of water [29]. When an energy deposition occurred within 6 Å of any DNA molecule, the energy deposited was assigned to the closest molecule sugar, phosphate or base molecule. Following previous work, an SSB was considered to occur if 17.5 eV of energy was assigned to a sugar-phosphate moiety [30]. This same work considers a sensitive volume around the sugar-phosphate moiety of $0.573\,\mathrm{nm}^3$, closely matched by the 6 Å limit we choose when considering energy depositions (which implies a sensitive volume of $0.596\,\mathrm{nm}^3$). Physically, a 6 Å limit corresponds to an implicit assumption that ionisation and excitation within any of the three hydration shells of B-DNA can contribute to physical damage, noting that the third hydration shell, ending near 6.5 Å from the DNA chain is important in maintaining the structure of B-DNA through hydrogen bonds [31]. The DNA molecules were considered to be liquid water for the purposes of physics modelling. The cross sections of the four bases and the sugar phosphate backbone are significantly different to water [32,33], however this level of modelling is outside the scope of this work.

2.2. Chemistry

Chemistry was simulated using a re-implementation of Geant4-DNA's chemistry module, built around the Independent Reaction Times (IRT) model, rather than the step-by-step approach currently available in the public release [34,35]. Both the IRT model and the dynamical step-by-step approach are event-based simulations, however they differ in the choice of events to consider. In the IRT approach [36], an event is a reaction between a pair of reactants. In the dynamical SBS approach, an event is defined by a species leaving its protective sphere, defined both in time and in space. While the second approach is slightly more accurate, the IRT method is significantly faster as it completes in fewer time steps. Chemistry was further accelerated by only considering molecules within $r_{\mathrm{kill}} = 4\,\mathrm{nm}$ of the DNA chain for simulation, where r_{kill} is the distance from DNA at which radical tracks were killed. Given scavenger densities in nuclei, radicals further than this from DNA are likely to be scavenged before they can react with DNA. For selected energies, we re-ran our simulations only simulating radicals created within $r_{\mathrm{kill}} = 1\,\mathrm{nm}$ of DNA, replicating hypothesised cellular conditions where only non-scavengeable radicals created in the hydration shells can cause indirect cellular damage [37,38].

Initial radicals were seeded in a physicochemical stage, which transports electrons having less then 8 eV (where physical tracking stops) down to thermalisation, as well as determining the dissociation channels followed by excited and ionised water molecules. The default Geant4-DNA dissociation channels have been kept for this simulation. After the physico-chemical stage, chemical reactions were simulated using the IRT model and the default Geant4 reaction and diffusion rates. The chemical stage was stopped after 1 ns, as after this time, > 95% of radicals within the regions simulated had reacted.

Reactions were simulated between the ˙OH, H˙, and e_{aq} radicals and the sugar-phosphate group (deoxyribose 5-phosphate) of DNA, and the bases guanine, adenine, cytosine and thymine, using previously reported reaction rates (Table 1). The overwhelming majority of reactions occur between the sugar-phosphate group and ˙OH, and between the bases and ˙OH or e_{aq}. The efficiency with which the reaction between ˙OH and the sugar-phosphate moiety induced a SSB was set to 40%, causing around 13% of all reactions between DNA and ˙OH to induce a double strand break, in agreement with previous experimental studies and simulations [39,40]. Reaction rates and diffusion constants for the remaining radicals were unchanged from the Geant4-DNA default rates.

2.3. Geometry

We modelled the full genome of an *E. coli* cell in Geant4, effectively simulating the bacterial nucleolus as an ellipsoid with a long semi-major axis of 950 μm and two short semi-major axes of 400 μm. A general particle source with the same dimensions was placed around this region. DNA was placed in the cell following a space-filling Hilbert curve, that was broken up into curved and straight placement volumes (Fig. 1). Each placement volume contained four straight or turned DNA segments (Fig. 2), modelled upon the structure of B-DNA. Each base pair of the DNA chain was modelled as six independent molecules, either sugar, phosphate or a nucleobase, with their position coming from the radially weighted mean position of their constituent molecules [41]

Table 1
Reaction rates used between radicals and DNA components ($\times 10^9\,\mathrm{L\,mol}^{-1}\,\mathrm{s}^{-1}$), from Buxton et al. [58].

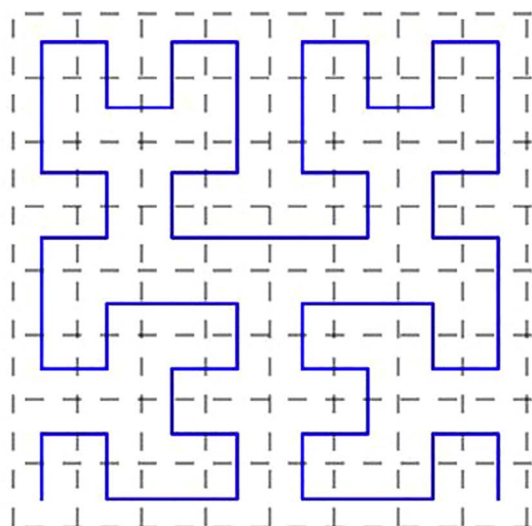|	˙OH	H˙	e_{aq}
$C_6H_5O_6P$	1.8	0.029	0.01
Adenine	6.1	0.10	9.0
Thymine	6.4	0.57	18.0
Guanine	9.2	–	14.0
Cytosine	6.1	0.092	13.0

Fig. 1. The overall geometry of the DNA chain is defined by a 1-D space filling curve. This fractal curve is broken into turned and straight regions, which correspond to turned and straight sections of DNA.
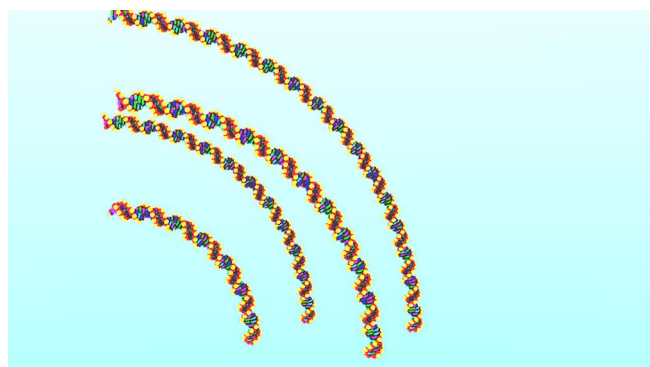

Fig. 2. An example turned segment of DNA. Each placement of DNA contains 4 strands.

Table 2
Semi-Major x, y and z axes (a, b and c respectively) of molecules modelled in the application.

Molecule	a (Å)	b (Å)	c (Å)	Volume (Å³)
Phosphate	2.28	2.28	2.28	49.8
Deoxyribose	2.63	2.63	2.63	76.4
Guanine	3.63	3.80	1.89	109.1
Cytosine	3.60	3.07	1.78	82.2
Thymine	4.21	3.04	2.00	107.3
Adenine	3.43	3.74	1.93	103.9

and their radii representing the radius required to give an equivalent volume as that derived from the summed van der Waal's radii of each constituent atom (subtracting overlaps), as indicated in Table 2. All structures were modelled physically as containing water.

A Hilbert curve was used to determine the placements of each sub-volume, as DNA follows a fractal curve structure at large scales, ensuring that linearly close genes on the DNA strand are also spatially close [42,43]. Our Hilbert curve was iterated 4 times, and three Hilbert curves were placed end to end to fill the entire cellular ellipsoid. Sections of the curve that would have fallen outside of the defined nucleolus region were not placed, leaving a geometry with 4.63 Mbp, matching *E. coli* (Fig. 3). Removing placement volumes that fall outside of the elliptical region we consider does break the continuity of the
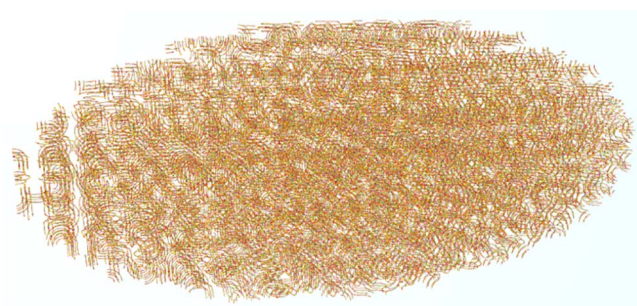

Fig. 3. We consider DNA in our *E. coli* geometry to be packed into an ellipsoid. As the fractal geometry we generate is square, it is cut where it exceeds the boundaries of the ellipse, leaving some loose ends.

DNA strands we model, however the impact of this on measured SSB and DSB yields is minimal, as the model remains 'mostly connected'.

2.4. Damage classification

We have classified the damage induced in DNA segments by both complexity and source, following the classification scheme of Nikjoo et al. [39]. Fig. 4 summarises this scheme, and is based on two parameters, d_{DSB} (typically set to ten), which is the maximum separation between two break events, on opposite sides of the DNA chain, for their correlated damage to be considered a DSB, and d_S, the length of undamaged base pairs required for two damaged segments to be considered independently (we consider that $d_s = 100$ bp). Once a segment has a DSB occur on it, it will be classified into one of the categories of DSBs, regardless of the number of SSBs also present. The classification DSB+ requires that in addition to a DSB, a base pair span have at least two breaks on one strand within the same d_{DSB}. The DSB++ classification requires that a damaged segment have at least two DSBs. The classification by source when DSBs are present differentiates the multiple roles indirect damage can have on causing a DSB. When the DSBs on the strand are only due to direct effects, a DSB_d occurs, and a DSB_i occurs when only indirect effects are present. When mixed damage is present, the segment is classified as DSB_m, except in the DSB_{hyb} case, which occurs when the break would be an SSB were indirect damage not included.

In this work, we also consider total yields of SSBs or DSBs that occur. Total yields are calculated by considering the sum of the total number of SSBs that occur, amongst the SSB classifications (as the classifications SSB+ and 2SSB can correspond to two or more SSBs). The total yield of DSBs is calculated as the sum of the number of DSB and DSB+ classifications, added to double the number of segments classified as DSB++.

2.5. Summary of simulation parameters

The parameters used in our simulations are summarized in Table 3. These parameters were derived and justified in Part 1 of this study [1]. The cellular geometry was irradiated with electrons having energies between 1 and 990 keV and with protons having energies ranging from 500 keV to 30 MeV. To achieve good statistical convergence, the number of events was chosen so that both a minimum total energy of at least 10 MeV was deposited in each cell, and at least 100 DSBs were recorded. Each simulation was repeated a second time, using $r_{kill} = 1$ nm. As this decreased the likelihood of a DSB occurring, we often doubled the number of events so that over 100 DSBs occurred.

Primary particles were created from the surface of the same 950 μm × 400 μm × 400 μm ellipse that enclosed the DNA geometry. They were seeded with a cosine angular distribution, which simulates an isotropic radiation environment. As some of our results show LET rather than the electron or proton energy as the dependent variable, we
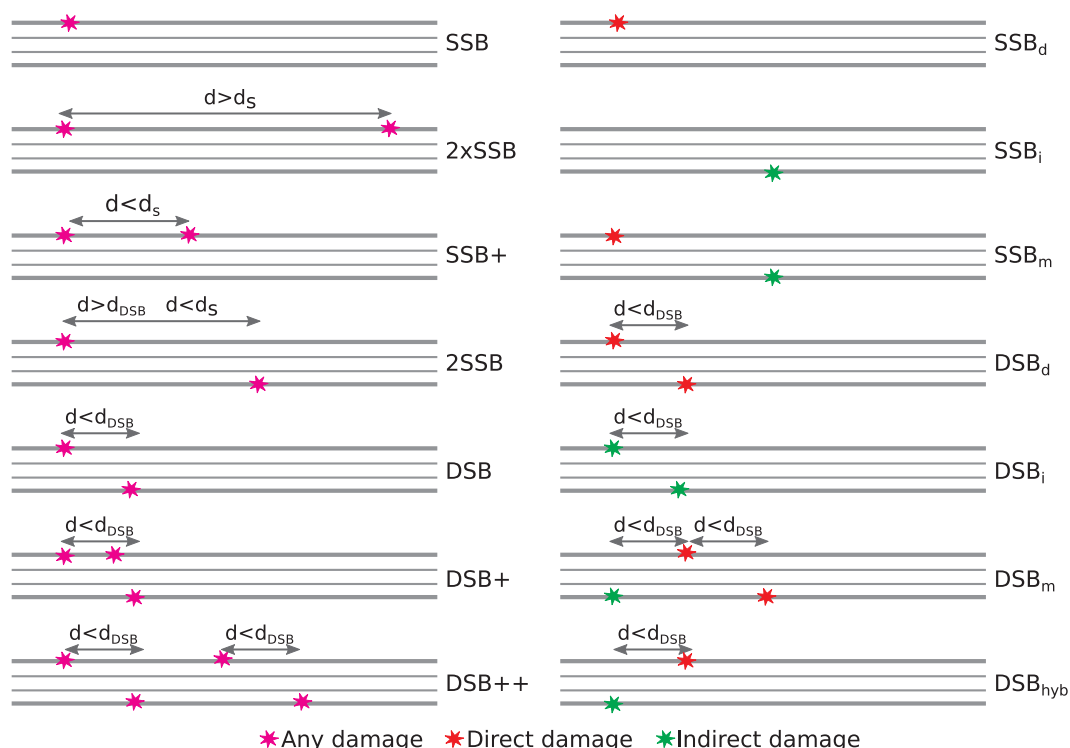
Fig. 4. DNA damage is classified according to the scheme originally proposed by Nikjoo et al., 1997 (discussed in text).

calculated the LET based on the ratio of the average energy deposited in the cell by the incident particle to the average chord length of this ellipsoidal region. LET was only considered for protons and electrons having an initial energy greater than or equal to 40 keV, as otherwise the LET varied too greatly as the particle traversed the cell.

3. Results

In order to benchmark our code against previous works, we consider the number of strand breaks induced in both the PARTRAC code [44], and in the code developed in M16, a previous DNA damage simulation made using Geant4-DNA [7]. Both these codes consider the irradiation of a human fibroblast cell by protons. Under irradiation from 10 MeV protons, we find that our code produces slightly more indirect breaks than PARTRAC, and noticeably fewer breaks than M16's work (Fig. 5). Our direct break yields are slightly higher than those found in M16, which uses the same 17.5 eV threshold for determining physical damage induction, and noticeably less than those found by PARTRAC. The threshold for direct damage in PARTRAC is a linearly varying probability ranging from 5 eV to 37.5 eV. When considering this threshold in simulation, the yield of SSBs increases by about 0.03 SSB Gy^{-1} Mbp^{-1}, significantly improving the agreement between the direct and total DSB yields with PARTRAC. Considering a range of LETs, we observe a globally good agreement in the total number of SSBs found in this work

compared to PARTRAC (Fig. 6), though physical damage is lower than PARTRAC would suggest due to our differing consideration of physical damage induction. At very high LETs, indirect damage drops off significantly in the PARTRAC models, a behaviour that is not echoed as strongly using Geant4-DNA, while under electron irradiation, we find more indirect damage than PARTRAC does.

Measurements of DSB yields in *E. coli* following X-irradiation find yields between 0.002 and 0.010 DSB Gy^{-1} Mbp^{-1} [45–47]. These are largely in agreement with the range of DSB yields we simulate for electron irradiation (Fig. 7). Simulating only radicals within 1 nm of DNA, whilst a departure from previous simulation methodologies, simulates well the lower end of the experimentally determined DSB

Table 3
Simulation parameters that best match Nikjoo et al., 1997 [39].

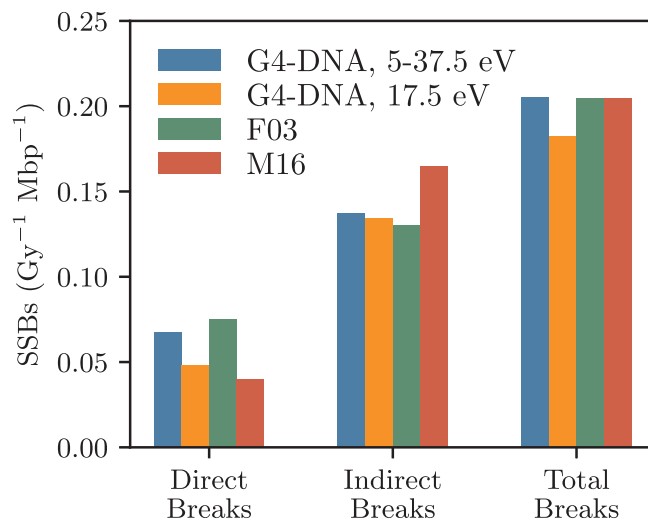| Parameter	Description	Value
E_{low}	Lower limit for physical damage	17.5 eV
E_{high}	Upper limit for physical damage	17.5 eV
r_{phys}	Radius for direct damage	Å
d_{DSB}	Distance between SSBs for DSB	10 bp
r_{kill}	Distance from DNA to kill radicals	4 nm
p_{SSB}	Pr($\cdot$OH + C$_6$H$_5$O$_6$P $\rightarrow$ SSB)	0.4
–	Simulation End Time	1 ns
–	Max. IRT time step	500 ps

Fig. 5. The total number of breaks induced by 10 MeV protons compares well to data from the PARTRAC (F03, follows 5–37.5 eV model [44]) and a past Geant4-DNA based work (M16, follows 17.5 eV model [7]) simulation platforms, with the differing energy threshold for induced breaks causing the majority of the difference between the direct break yields.
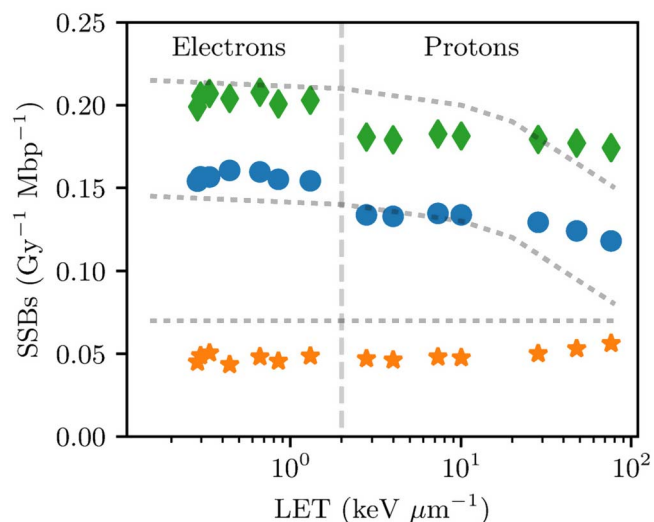
Fig. 6. Total yields for direct (stars), indirect (circles) and all (diamonds) SSBs in Geant4-DNA. We tend to slightly underestimate the damage yields seen in PARTRAC (horizontal lines, [44]), in part due to an underestimation of direct damage. A vertical line separates proton and electron data.

Fig. 8. The ratio of SSBs to DSBs is plotted for different values of r_{kill} across the range of electron energies studied. The comparison data, from both simulation and experiments in plasmids, is the same as in Fig. 7.

yields, while simulating radicals out to 4 nm simulates well the upper end of experimental yields measured. No experimental yields of SSBs in *E. coli* exist, due to measurement difficulties, however measurements of SSB and DSB yields in plasmids, and break yields from other simulation platforms, can serve as a useful point of comparison (whilst bearing in mind that there are geometrical differences between the simulations). Simulations of DNA damage from electron irradiation broadly show a better agreement with the 4 nm data, as do measurements of SSB and DSB yields in plasmids. DSB measurements in plasmids are typically noisy, with an experimental error on the order of 0.003 DSB Gy^{-1} Mbp^{-1} [48].

The ratio of SSBs to DSBs is a robust measure that should be largely independent of the differences between experimental and simulation geometries. For electron energies below 10 keV, we find excellent agreement between experimental and simulated SSB/DSB values [49],
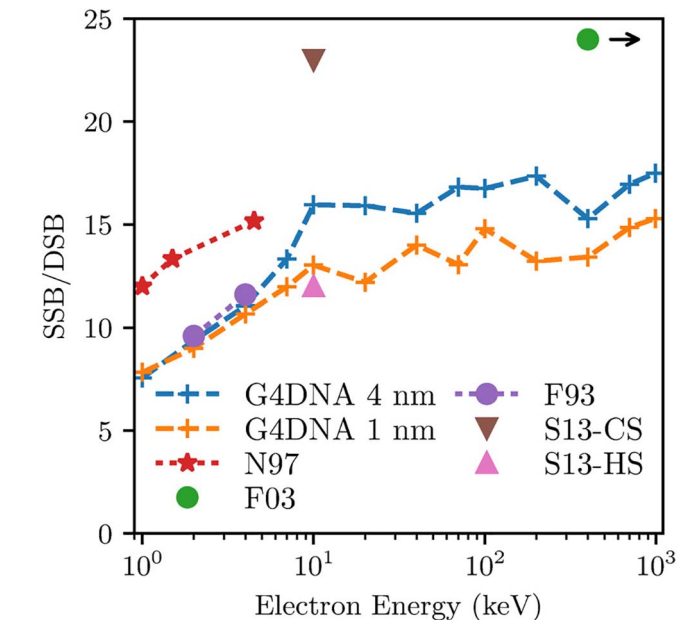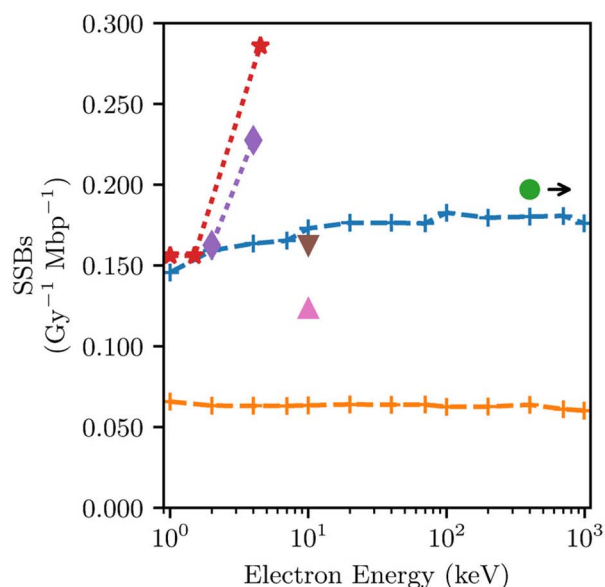
whilst finding a value lower than other simulations across the entire range of measurements made (Fig. 8). X-ray data at 4 keV μm^{-1} (near the LET of 10 keV electrons) replicates well the SSB/DSB ratio of 10 keV electrons in a high scavenging regime, while a lower scavenging concentration more representative of radical scavenging in the absence of folding proteins suggests we significantly underestimate the SSB/DSB ratio. At higher energies, we find that the ratio of SSBs to DSBs converges to 17 based on our parameter set, or to 15 when only radicals close to DNA are simulated.

When proton damage is considered (Fig. 9), we better reproduce the results of other simulations when radicals are simulated out to 4 nm. As seen for electrons, simulating only non-scavengeable radicals created very close to DNA greatly decreases the SSB and DSB yields, however it
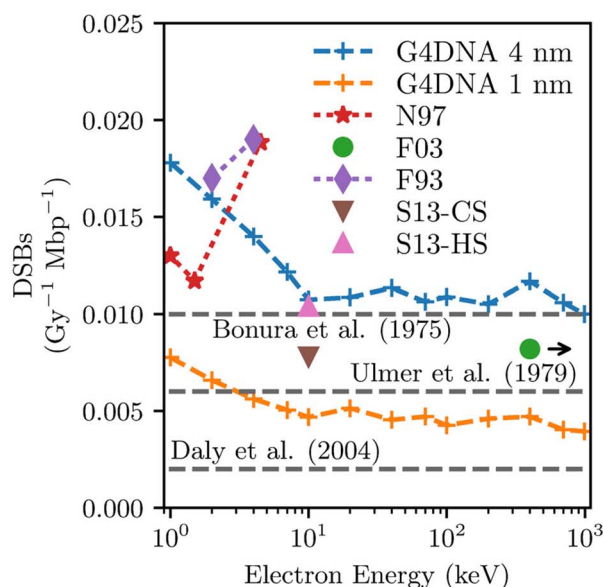
Fig. 7. SSB and DSB yields from electrons, considering both a 1 nm and 4 nm radius from DNA for radical interactions. Both figures share the same legend. N97 [39] and F03 [44] refer to simulation data (F03 consider 30 MeV electrons, indicated by arrows), while F93 [49] and S13 [59] come from plasmid data. Cellular (CS: 3×10^8 s^{-1}) and higher (HS: 1×10^{10} s^{-1}) scavenger densities are plotted for the S13 data, where damage is induced by 4 keV μm^{-1} X-rays (similar LET to 10 keV electrons). The grey parallel lines in the right-hand panel show measured DSB yields in *E. coli* following X-irradiation.

Fig. 9. SSB and DSB yields from proton damage measured using Geant4-DNA, compared to results from the PARTRAC (F03) simulation platform [44], and the KURBUC (N01) code [50]. Experimental DSB yields are indicated by F99 for human fibroblast cells [60], and B00 for V79 Chinese Hamster cells [61].
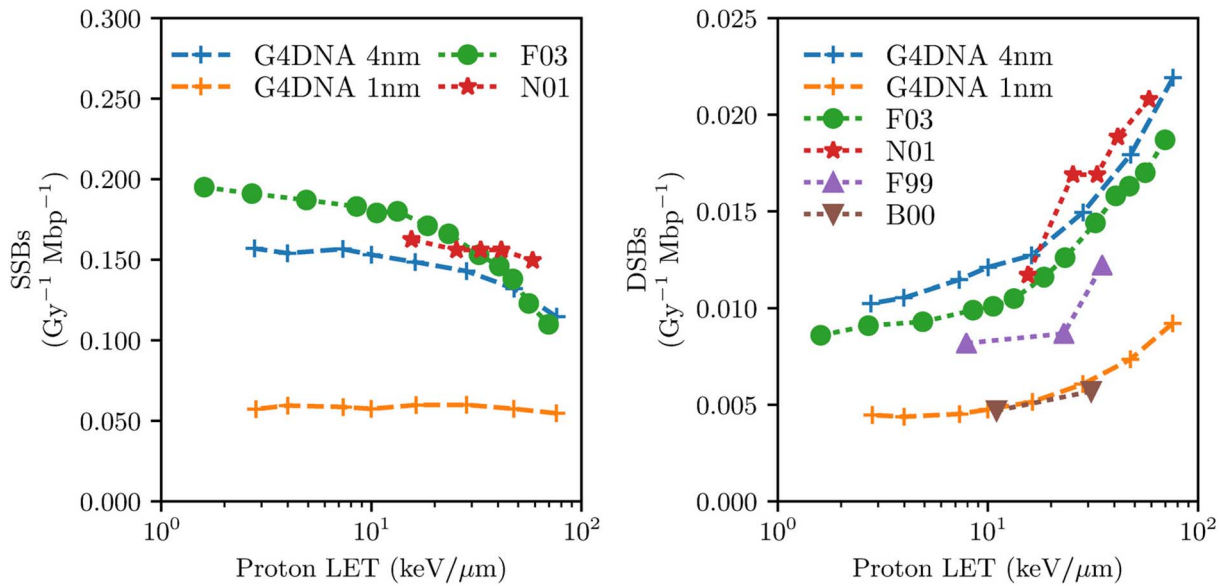
only minimally affects the ratio of SSBs to DSBs (Fig. 10). By changing the simulation of scavenging however, the yields of strand breaks can double, illustrating the sensitivity of our simulation on how this process is modelled. A priori, we can see no difference why the two cell experimental measurements considered in Fig. 9 should show a dependence upon scavenging efficiency, yet changing this parameter allows the range of experimental results we consider to be modelled. While at high LETs, we reproduce the SSB/DSB ratio measured in other simulations, the lower quantity of SSBs we measure compared to the PARTRAC and KURBUC simulation platforms leads to a corresponding underestimation of this ratio. More noticeable though is the large underestimation by all simulation platforms of the SSB/DSB ratio observed in experimental measurements in plasmids using proton sources. This difference is less apparent when considering electron damage.

As LET increases, we expect the complexity of breaks to increase. Fig.11 shows the ratio of complex SSBs (ie. SSB+ and 2SSB) and complex DSBs (ie. DSB+ and DSB++) to total SSBs and DSBs as LET increases, indicating a clear increase in the proportion of complex breaks as LET increases (electrons with energies less than 40 keV are not shown in Fig. 11, as the LET changes is highly variant within the cell). This is in line with observations of protein recruitment seen in microbeam-irradiated cells, though the fractions of complex breaks we report are lower than those seen in other simulation studies [50]. For both electrons and protons, increasing the LET increases the fraction of complex breaks (Fig. 12), as expected.

This work falls within the scope of a larger study that seeks to classify the mutational impact of background radiation on *E. coli* [10]. In this past work, we showed that the median energy deposited in a cell by most sources of background radiation is around 140 eV ($\approx$ 10 mGy in the geometry used), and that *E. coli* cells are struck by background radiation with a probability of 6×10^{-5} day^{-1}. Most electrons coming from the background that interact with bacterial cells have energies of 10 keV and above, and according to our results here will induce approximately 0.01 DSB Gy^{-1} Mbp^{-1}. Combining these estimates, a median estimate for the number of ionising radiation induced strand breaks caused per day in an *E. coli* is 2.8×10^{-8} DSB day^{-1}. This strengthens the conclusions of the previous works we have conducted in this domain that suggest that while ionising radiation from the natural background does cause DNA damage, its effects are negligible compared to mutations that come from sources endogenous to the cell.
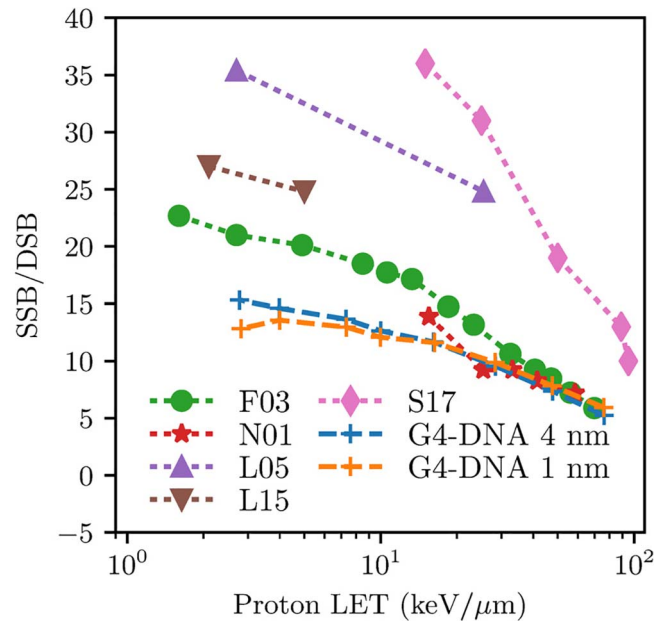

Fig. 10. The SSB/DSB ratio is shown for the simulation data sets presented in Fig. 10, alongside SSB/DSB ratios measured in plasmids, indicated by, L05 [62], L15 [63] and S17 [64]. The fractional uncertainty for each plasmid measurement is often as large as 30%.

4. Discussion

This work represents the first effort to develop a single Geant4 application that can model direct and indirect DNA damage in a continuous geometry. Here, we consider the geometry of an *E. coli* cell, following from a previous work that sought to quantify the mutational role of background radiation. Despite considering a bacterial DNA geometry, where DNA does not pack into chromatin as is seen in human cells, we have compared our data to works that simulate human cells, and to damage measurements from plasmids, animal and bacterial cells. We begin therefore by addressing the questions these comparisons raise regarding simulation geometries. Next, we discuss our results in relation to other simulations and experimental results. A brief perspective is offered regarding the role of works such as this one in relation to low
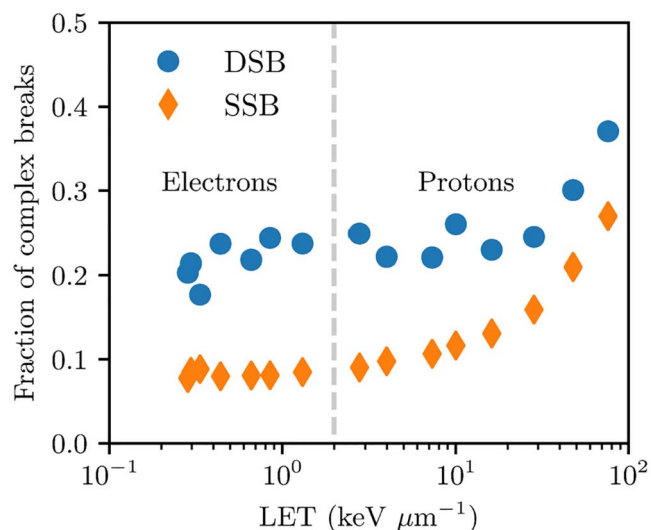
Fig. 11. As the LET of incident radiation increases, the complexity of stand breaks also increases.

dose radiation studies, before we highlight some of the further ways mechanistic DNA damage simulations can be expanded.

Previous simulation studies have focused on cellular geometries with varying levels of realism, from random straight chords [39,50] to disjoint chromosomal segments [51,52] to full cells [2,4,7]. Recent work has been conducted to generate tools that can procedurally generate different cell types for simulation [6], suggesting that the cell type could have a large bearing on mechanistic damage simulations, however the similarity of results between multiple geometries suggests that these differences are negligible, especially when viewed in relation to the differences in damage yields that come from slightly changing the damage model. By and large, cell geometry dependent differences in strand break yield should be negligible because strand break yields are normalised by the radiation dose and the number of base pairs considered, which is equivalently a normalisation by the density of base pairs and the energy deposited in a cellular region. As, at the scale of a

strand break, most continuous DNA strands are similar, damage yields should not show a strong dependence on geometry, meaning our bacterial model ought to be comparable to chromatin-based data. We note though that randomly placing short segments of DNA can increase damage yields due to a lack of spatial correlation in the DNA. This is observed in Part 1 [1] which examined a random packing of 216 bp long DNA segments, finding DSB yields two to three times higher than what has been observed here. As plasmids are randomly packed to some extent, we only emphasise our comparisons to plasmid data when considering SSB/DSB, as the raw yields of SSBs and DSBs may be influenced by the random orientations of discrete plasmids. Further geometrical studies examining the role to which spatial correlations can influence DNA damage could be of interest, however we expect only minor differences would be observed when passing from individual DNA strands to chromatin, as at the scale of a DSB (10 bp), the geometries are quite similar.

The total number of direct and indirect breaks provides a simple way to compare simulation platforms independent of what constitutes a DSB. Similar SSB yields are seen from both direct and indirect sources as that observed in PARTRAC and M16. By changing the energy threshold for bond breakages, we produce direct SSB yields concordant with each of the two platforms. Results obtained however by H. Nikjoo's group [39,50] often tend to show that direct damage dominates indirect damage, in contrast to the observations made here, despite using a 17.5 eV threshold for physical damage (the same as this work). The similarities between our work and the PARTRAC and M16 works likely comes from a shared model for the implementation of chemistry, as the chemistry module in Geant4-DNA was influenced in its early stages by PARTRAC [53]. That indirect effects dominate SSB formation is consistent with experimental results, especially at low LET [54], though consideration of only non-scavengeable radicals can reduce this fraction to produce direct and indirect SSB yields more in line with the work of Nikjoo. More broadly, across the LETs considered in this work, we reproduce the trends observed by PARTRAC with some small variation (Fig. 6). Relative to PARTRAC, we underestimate direct damage, due to our use of a fixed 17.5 eV damage threshold, while at high LET, simulations conducted in PARTRAC exhibit a steeper drop in indirect damage than we observe. Only a slight drop in indirect damage yields is seen in M16, suggesting that this difference between Geant4-
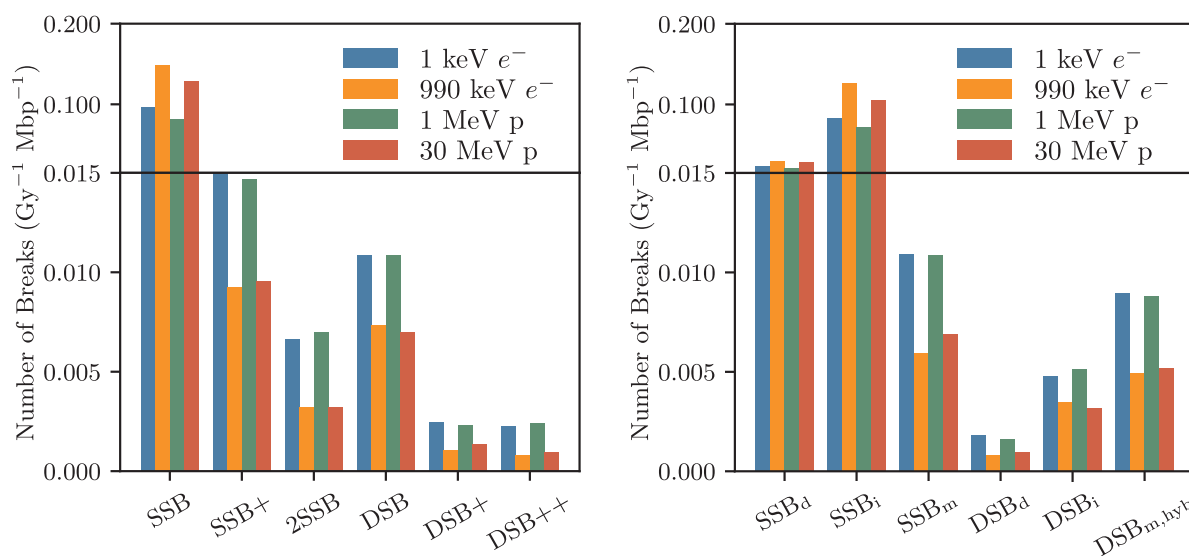

Fig. 12. Breaks by complexity and source, showing that high LET radiation causes in general more chemical damage, and more complex breaks. A horizontal line occurs where we have broken the y-axis for clarity.

DNA based simulations of indirect damage and PARTRAC is not linked to approximations in how the chemistry is calculated (as M16 uses discrete time-steps with a Brownian bridge in the chemical phase of the simulation, while we use the IRT method). Our ratios of SSB to DSB damage correspond well to recent simulations by Nikitaki et al. [55] who also consider electrons with energies below that considered here, recovering a peak in DSBs near incident electron energies of 300 eV, echoing what we observed in Part 1 of this study [1].

A range of experimental data exists for DSB yields in *E. coli* induced by X-rays. As X-rays mainly damage DNA through the low energy electrons they create via Compton scattering and photoelectric absorption, this data is very roughly comparable to the DSB yields we measure from electron damage in DNA. For electrons with energies above 10 keV, the DSB yields we measure are comparable to those measured in *E. coli*, however the experimental data is dispersed across a large range (0.002–$0.010 \, \mathrm{DSB \, Gy^{-1} \, Mbp^{-1}}$), which covers a similar magnitude to the errors likely induced by approximations in our models. The modelling of scavenging remains one such poorly resolved model parameter. A value of $r_{\mathrm{kill}} = 4$ nm provides a reasonable agreement with simulated SSB and DSB yields, however simulation of radicals within the hydration shells of DNA ($r_{\mathrm{kill}} = 1$ nm) better matches the range of experimental measurements observed, as well as better reproducing SSB/DSB ratios from plasmids when high scavenger concentrations are present (Fig. 8). Better incorporation of the SSB/DSB ratio when comparing mechanistic simulations to experiments allows the assumptions in our models to be better tested, however this is difficult as SSB yields cannot be calculated in plasmids. Our suggestion that r_{kill} should be 1 nm may even be an overestimate, as the third hydration shell of DNA, within which unscavengeable radicals are created, ends 6.5 Å from the DNA [31].

When considering proton damage, SSB and DSB yields are again similar to past simulation works when $r_{\mathrm{kill}} = 4$ nm, though we observe a better agreement with some experimental yields when $r_{\mathrm{kill}} = 1$ nm (Fig.9). The reduced SSB yield when $r_{\mathrm{kill}} = 1$ nm could be a good way of discriminating between the best ways to simulate scavenging. When the SSB/DSB ratio is considered however, experimental comparisons leave us with very few clues as all plasmid data indicates SSB to DSB ratios significantly higher than those predicted by simulation when proton damage is considered (Fig. 10). It is possible that under proton irradiation, the plasmids are more susceptible to chemical damage from distant radicals, due to the lack of folding proteins. Attacks from diffusing radical species may lead to a significantly higher yield of chemically induced SSBs. This would be consistent with all simulations under-estimating the SSB/DSB ratio compared to experiments across all LET's considered.

As LET measures the density of energy depositions, it is expected that at high LETs, DNA damage becomes more complex. A rise in complex damage can be seen beyond LET's of 3–5 keV $\mu\mathrm{m}^{-1}$ (Fig. 11), which corresponds to energy deposits of around 10–20 eV in a 3.4 nm (10 bp long) linear region. The link between LET and break complexity is also seen in our strand break classifications (Fig. 12), where LET can be seen to be a more significant factor in determining break complexity than the source of radiation. Interestingly though, low LET radiation favours the formation of many indirect SSBs, both a consequence of high LETs often leading to more complex damage, and the decreased likelihood of direct SSBs in low LET irradiation leaving radical attack to be a more dominant vector for DNA damage to occur.

From these results, we can begin to assemble a picture of how the radiation background damages DNA. The frequency distribution of energy depositions from the background in cells tends to follow a Landau distribution. This means that very large amounts of energy can be deposited by background radiation in cells (often more than 1 keV), however these depositions are rare compared to the median energy deposition (100–200 eV). Such small total energy deposits, which correspond to around ≈ 10 mGy already have only a very small chance of causing a DSB or SSB in *E. coli*, given its relative short genome and the

yields we have simulated here. In a previous work, we suggested that the low rate at which charged particles caused by the natural radiation background enter cells ($6 \times 10^{-5} \, \mathrm{day}^{-1}$ in a surface laboratory) makes it difficult to draw a link between the radiation background and mutations [10], as the mutation rate from endogenous causes is orders of magnitude higher ($10^{-3} \, \mathrm{division}^{-1}$) than the rate at which the background interacts with cells. Nevertheless, it may have been possible for radiation to have rare, catastrophic results that induce mutations. By showing in this work that the DSB rate from the background in a cell is again very small, we challenge this hypothesis. Rather responses observed in cellular systems subjected to reductions in the radiation background likely originate from cell communication [19,56] or regulatory changes induced in the cell linked to radiation [18,57].

5. Conclusion

We have presented, using the same generic application framework as Part 1 of this study, mechanistic DNA damage measurements from electrons and protons in *E. coli*. A reasonable agreement with experiment was observed for DSB yields from protons and electrons, however a key question to be confronted in future works is the simulation of scavenging. We have shown that only simulating non-scavangeable radicals, that is radicals created near DNA's hydration shells can sometimes reproduce experimental results better than current practices for the simulation of scavenging, however targeted experiments and simulations are needed to better address this.

When comparing our results to previous simulations, we found that the different cellular geometries considered by authors do not seem to greatly affect the yields of SSBs and DSBs. This is consistent with observations of a near-constant DSB yield rate in across many cell types [37]. Further work, simulating DNA damage yields in different cell geometries with the same simulation platform would strengthen this finding.

We used our simulations to predict the impact of the radiation background on the DSB rate, finding that for a given cell, the natural radiation background near the surface is responsible for $2.8 \times 10^{-8} \, \mathrm{DSB \, day}^{-1}$. While we cannot directly convert the DSB rate to the radiation induced mutation rate, this does indicate that the radiation background likely has only a very small mutational effect on systems, and that the mutation rate in biological systems is dominated by those that come from endogenous sources, such as transcription errors. This is an important conclusion for biological studies at low backgrounds, as it effectively suggests that the radiation background has a negligible impact on the supply rate of mutations.

References

[1] Lampe N, Karamitros M, Breton V, Brown JMC, Sakata D, Sarramia D, et al. Mechanistic DNA damage simulations in geant4-DNA Part 1: a parameter study in a simplified geometry. Phys Med 2017. submitted for publication.

[2] Nikjoo H, Girard P. A model of the cell nucleus for DNA damage calculations. Int J Radiat Biol 2012;88:87–97. http://dx.doi.org/10.3109/09553002.2011.640860.

[3] Nikjoo H, Uehara S, Emfietzoglou D, Cucinotta FA. Track-structure codes in radiation research. Radiat Meas 2006;41:1052–74. http://dx.doi.org/10.1016/j.radmeas.2006.02.001.

[4] Friedland W, Dingfelder M, Kundrát P, Jacob P. Track structures, DNA targets and radiation effects in the biophysical Monte Carlo simulation code PARTRAC. Mutat Res 2011;711:28–40. http://dx.doi.org/10.1016/j.mrfmmm.2011.01.003. Elsevier B.V.

[5] Friedland W, Schmitt E, Kundrát P, Dingfelder M, Baiocco G, Barbieri S, et al. Comprehensive track-structure based evaluation of DNA damage by light ions from radiotherapy-relevant energies down to stopping. Sci Rep 2017;7:45161. http://dx.doi.org/10.1038/srep45161. Nature Publishing Group.

[6] Meylan S, Vimont U, Incerti S, Clairand I, Villagrasa C. Geant4-DNA simulations using complex DNA geometries generated by the DnaFabric tool. Comput Phys Commun 2016;204:159–69. http://dx.doi.org/10.1016/j.cpc.2016.02.019. Elsevier B.V.

[7] Meylan S. Development of a multi-scale simulation tool for early radio-induced damage assessment in cells exposed to light ions irradiations (proton and alpha). Université de Bordeaux; 2016.

[8] Meylan S, Incerti S, Karamitros M, Tang N, Bueno M, Clairand I, et al. Simulation of

early DNA damage after the irradiation of a fibroblast cell nucleus using Geant4-DNA. Sci Rep 2017;7:11923. http://dx.doi.org/10.1038/s41598-017-11851-4.

[9] Nikjoo H, Taleei R, Liamsuwan T, Liljequist D, Emfietzoglou D. Perspectives in radiation biophysics: From radiation track structure simulation to mechanistic models of DNA damage and repair. Radiat Phys Chem Pergamon 2016;128:3–10. http://dx.doi.org/10.1016/j.radphyschem.2016.05.005.

[10] Lampe N, Biron DG, Brown JMC, Incerti S, Marin P, Maigne L, et al. Simulating the impact of the natural radiation background on bacterial systems: Implications for very low radiation biological experiments. PLoS ONE 2016;11:1–19. http://dx.doi.org/10.1371/journal.pone.0166364.

[11] Lampe N, Marin P, Castor J, Warot G, Incerti S, Maigne L, et al. Background study of absorbed dose in biological experiments at the Modane Underground Laboratory. EPJ Web Conf 2016;124:6. http://dx.doi.org/10.1051/epjconf/201612400006.

[12] Nikjoo H, Emfietzoglou D, Watanabe R, Uehara S. Can Monte Carlo track structure codes reveal reaction mechanism in DNA damage and improve radiation therapy? Radiat Phys Chem 2008;77:1270–9. http://dx.doi.org/10.1016/j.radphyschem.2008.05.043.

[13] El Naqa I, Pater P, Seuntjens J. Monte Carlo role in radiobiological modelling of radiotherapy outcomes. Phys Med Biol 2012;57:R75–97. http://dx.doi.org/10.1088/0031-9155/57/11/R75.

[14] Nikjoo H, Emfietzoglou D, Liamsuwan T, Taleei R, Liljequist D, Uehara S. Radiation track, DNA damage and response—a review. Reports Prog Phys 2016;79:116601. http://dx.doi.org/10.1088/0034-4885/79/11/116601. IOP Publishing.

[15] Elsässer T, Krämer M, Scholz M. Accuracy of the local effect model for the prediction of biologic effects of carbon ion beams in vitro and in vivo. Int J Radiat Oncol Biol Phys 2008;71:866–72. http://dx.doi.org/10.1016/j.ijrobp.2008.02.037.

[16] Brown JMC, Currell FJ. A local effect model-based interpolation framework for experimental nanoparticle radiosensitisation data. Cancer Nanotechnol 2017;8:1. http://dx.doi.org/10.1186/s12645-016-0025-6. Springer Vienna.

[17] Hawkins RB. A microdosimetric-kinetic model for the effect of non-Poisson distribution of lethal lesions on the variation of RBE with LET. Radiat Res 2003;160:61–9. http://dx.doi.org/10.1667/RR3010.

[18] Lampe N, Breton V, Sarramia D, Sime-Ngando T, Biron DG. Understanding low radiation background biology through controlled evolution experiments. Evol Appl 2017. http://dx.doi.org/10.1111/eva.12491.

[19] Castillo H, Schoderbek D, Dulal S, Escobar G, Wood J, Nelson R, et al. Stress induction in the bacteria Shewanella oneidensis and Deinococcus radiodurans in response to below-background ionizing radiation. Int J Radiat Biol 2015;3002:1–33. http://dx.doi.org/10.3109/09553002.2015.1062571.

[20] Castillo H, Smith GB. Below-background ionizing radiation as an environmental cue for bacteria. Front Microbiol 2017;8:1–7. http://dx.doi.org/10.3389/fmicb.2017.00177.

[21] Møller AP, Surai P, Mousseau TA. Antioxidants, radiation and mutation as revealed by sperm abnormality in barn swallows from Chernobyl. Proc Biol Sci 2005;272:247–53. http://dx.doi.org/10.1098/rspb.2004.2914.

[22] Smith JT, Willey NJ, Hancock JT. Low dose ionizing radiation produces too few reactive oxygen species to directly affect antioxidant concentrations in cells. Biol Lett 2012;8:594–7. http://dx.doi.org/10.1098/rsbl.2012.0150.

[23] Katz JI. Comment on Castillo et al. (2015). Int J Radiat Biol 2016. http://dx.doi.org/10.3109/09553002.2016.1135265. 3002: 1-2.

[24] Bernal MA, Bordage MC, Brown JMC, Davídková M, Delage E, El Bitar Z, et al. Track structure modeling in liquid water: a review of the Geant4-DNA very low energy extension of the Geant4 Monte Carlo simulation toolkit. Physica Med 2015:1–14. http://dx.doi.org/10.1016/j.ejmp.2015.10.087.

[25] Bordage MC, Bordes J, Edel S, Terrissol M, Franceries X, Bardiès M, et al. Implementation of new physics models for low energy electrons in liquid water in Geant4-DNA. Phys Med 2016;32:1833–40. http://dx.doi.org/10.1016/j.ejmp.2016.10.006.

[26] Incerti S, Douglass M, Penfold S, Guatelli S, Bezak E. Review of Geant4-DNA applications for micro and nanoscale simulations. Physica Med 2016:1187–200. http://dx.doi.org/10.1016/j.ejmp.2016.09.007. Elsevier.

[27] Lampe N. The long term impact of ionising radiation on living systems. Université Clermont Auvergne; 2017.

[28] Emfietzoglou D, Cucinotta FA, Nikjoo H. A complete dielectric response model for liquid water: a solution of the Bethe ridge problem. Radiat Res 2005;164:202–11.

[29] Kyriakou I, Incerti S, Francis Z. Technical Note: Improvements in geant4 energy-loss model and the effect on low-energy electron transport in liquid water. Med Phys 2015;42:3870–6. http://dx.doi.org/10.1118/1.4921613. American Association of Physicists in Medicine.

[30] Charlton DE, Humm JL. A method of calculating initial DNA strand breakage following the decay of incorporated 125I. Int J Radiat Biol 1988;53:353–65. http://dx.doi.org/10.1080/09553008814552501.

[31] Nakano M, Tateishi-Karimata H, Tanaka S, Tama F, Miyashita O, Sichi Nakano, et al. Local thermodynamics of the water molecules around single- and double-stranded DNA studied by grid inhomogeneous solvation theory. Chem Phys Lett 2016;660:250–5. http://dx.doi.org/10.1016/j.cplett.2016.08.032.

[32] Abril I, Garcia-Molina R, Denton CD, Kyriakou I, Emfietzoglou D. Energy loss of hydrogen- and helium-ion beams in DNA: calculations based on a realistic energy-loss function of the target. Radiat Res 2011;175:247–55. http://dx.doi.org/10.1667/RR2142.1.

[33] Garcia-Molina R, Abril I, Kyriakou I, Emfietzoglou D. Inelastic scattering and energy loss of swift electron beams in biologically relevant materials. Surf Interface Anal 2017;49:11–7. http://dx.doi.org/10.1002/sia.5947.

[34] Karamitros M, Mantero A, Incerti S, Friedland W, Baldacchino G, Barberet P, et al. Modeling radiation chemistry in the Geant4 toolkit. Prog Nucl Sci Technol 2011;2:503–8.

[35] Karamitros M, Luan S, Bernal MA, Allison J, Baldacchino G, Davidkova M, et al. Diffusion-controlled reactions modeling in Geant4-DNA. J Comput Phys 2014;274:841–82. http://dx.doi.org/10.1016/j.jcp.2014.06.011. Elsevier Inc.

[36] Green NJB, Pilling MJ, Pimblott SM, Clifford P. Stochastic modeling of fast kinetics in a radiation track. J Phys Chem 1990;94:251–8. http://dx.doi.org/10.1021/j100364a041.

[37] Daly MJ. Death by protein damage in irradiated cells. DNA Repair (Amst) 2012;11:12–21. http://dx.doi.org/10.1016/j.dnarep.2011.10.024. Elsevier B.V.

[38] Ljungman M, Nyberg S, Nygren J, Eriksson M, Ahnström G. DNA-bound proteins contribute much more than soluble intracellular compounds to the intrinsic protection against radiation-induced DNA strand breaks in human cells. Radiat Res 1991;127:171–6.

[39] Nikjoo H, O'Neill O, Goodhead T, Terrissol M. Computational modelling of low-energy electron-induced DNA damage by early physical and chemical events. Int J Radiat Biol 1997;71:467–83.

[40] Milligan JR, Aguilera JA, Ward JF. Variation of single-strand break yield with scavenger concentration for plasmid DNA irradiated in aqueous solution. Radiat Res 1993;133:151–7.

[41] Arnott S, Hukins DWL. Optimised parameters for A-DNA and B-DNA. Biochem Biophys Res Commun 1972;47:1504–9. http://dx.doi.org/10.1016/0006-291X(72)90243-4.

[42] Lieberman-Aiden E, van Berkum NL, Williams L, Imakaev M, Ragoczy T, Telling A, et al. Comprehensive mapping of long-range interactions reveals folding principles of the human genome. Science (80-) 2009.

[43] Fritsche M, Li S, Heermann DW, Wiggins PA. A model for Escherichia coli chromosome packaging supports transcription factor-induced DNA domain formation. Nucleic Acids Res 2012;40:972–80. http://dx.doi.org/10.1093/nar/gkr779.

[44] Friedland W, Jacob P, Bernhardt P, Paretzke HG, Dingfelder M. Simulation of DNA damage after proton irradiation. Radiat Res 2003;159. http://dx.doi.org/10.1667/0033-7587(2003) 159[0401:SODDAP]2.0.CO;2. 410–410.

[45] Daly MJ, Gaidamakova EK, Matrosova VY, Vasilenko A, Zhai M, Venkateswaran A, et al. Accumulation of Mn(II) in Deinococcus radiodurans facilitates gamma-radiation resistance. Science (80-) 2004;306:1025–8. http://dx.doi.org/10.1126/science.1103185.

[46] Ulmer KM, Gomez RF, Sinskey AJ. Ionizing radiation damage to the folded chromosome of Escherichia coli K-12: sedimentation properties of irradiated nucleoids and chromosomal deoxyribonucleic acid. J Bacteriol 1979;138:475–85.

[47] Bonura T, Town CD, Smith KC, Kaplan HS. The influence of oxygen on the yield of DNA double-strand breaks in X-irradiated Escherichia coli K-12. Radiat Res 1975;63:567–77.

[48] Souici M, Khalil TT, Boulanouar O, Belafrites A, Mavon C, Fromm M. DNA strand break dependence on Tris and arginine scavenger concentrations under ultra-soft X-ray irradiation: the contribution of secondary arginine radicals. Radiat Environ Biophys 2016;55:215–28. http://dx.doi.org/10.1007/s00411-016-0642-9. Springer, Berlin Heidelberg.

[49] Folkard M, Prise KM, Vojnovic B, Davies S, Roper MJ, Michael BD. Measurement of DNA damage by electrons with energies between 25 and 4000 EV. Int J Radiat Biol 1993;64:651–8. http://dx.doi.org/10.1080/09553009314551891. Taylor & Francis.

[50] Nikjoo H, O'Neill P, Wilson WE, Goodhead DT. Computational approach for determining the spectrum of DNA damage induced by ionizing radiation. Radiat Res 2001;156:577–83. http://dx.doi.org/10.1667/0033-7587(2001) 156[0577:CAFDTS]2.0.CO;2.

[51] Friedland W, Bernhardt P, Jacob P, Paretzke HG, Dingfelder M. Simulation of DNA damage after proton and low LET irradiation. Radiat Prot Dosim 2002;99:99–102.

[52] Dos Santos M, Villagrasa C, Clairand I, Incerti S. Influence of the DNA density on the number of clustered damages created by protons of different energies. Nucl Instrum Methods Phys Res Sect B Beam Interact Mater Atoms 2013;298:47–54. http://dx.doi.org/10.1016/j.nimb.2013.01.009.

[53] Karamitros M. Extension de l'outil Monte Carlo généraliste Geant4 pour la simulation de la radiolyse de l'eau dans le cadre du projet Geant4-DNA. Université de Bordeaux; 2013.

[54] Hirayama R, Ito A, Tomita M, Tsukada T, Yatagai F, Noguchi M, et al. Contributions of direct and indirect actions in cell killing by high-LET radiations. Radiat Res 2009;171:212–8.

[55] Nikitaki Z, Nikolov V, Mavragani IV, Mladenov E, Mangelis A, Laskaratou DA, et al. Measurement of complex DNA damage induction and repair in human cellular systems after exposure to ionizing radiations of varying linear energy transfer (LET). Free Radic Res 2016;50:S64–78. http://dx.doi.org/10.1080/10715762.2016.1232484.

[56] Castillo H, Schoderbek D, Dulal S, Escobar G, Wood J, Nelson R, et al. Response to Dr Katz. Int J Radiat Biol 2016;92:169–70.

[57] Fratini E, Carbone C, Capece D, Esposito G, Simone G, Tabocchini MA, et al. Low-radiation environment affects the development of protection mechanisms in V79 cells. Radiat Environ Biophys 2015;54:183–94. http://dx.doi.org/10.1007/s00411-015-0587-4.

[58] Buxton GV, Greenstock CL, Helman WP, Ross AB. Critical review of rate constants for reactions of hydrated electrons, hydrogen atoms and hydroxyl radicals (OH/O) in Aqueous Solution. J Phys Chem Ref Data 1988;17:513–886. http://dx.doi.org/10.1063/1.555805.

[59] Shiina T, Watanabe R, Shiraishi I, Suzuki M, Sugaya Y, Fujii K, et al. Induction of DNA damage, including abasic sites, in plasmid DNA by carbon ion and X-ray irradiation. Radiat Environ Biophys 2013;52:99–112. http://dx.doi.org/10.1007/s00411-012-0447-4.

[60] Frankenberg D, Brede HJ, Schrewe UJ, Steinmetz C, Frankenberg-Schwager M, Kasten G, et al. Induction of DNA double-strand breaks by 1 H and 4 He ions in

primary human skin fibroblasts in the LET range of 8 to 124 keV/μm. Radiat Res 1999;151:540–9.

[61] Belli M, Cherubini R, Dalla Vecchia M, Dini V, Moschini G, Signoretti C, et al. DNA DSB induction and rejoining in V79 cells irradiated with light ions: a constant field gel electrophoresis study. Int J Radiat Biol 2000;76:1095–104. http://dx.doi.org/10.1080/09553000050111569.

[62] Leloup C, Garty G, Assaf G, Cristovão A, Breskin A, Chechik R, et al. Evaluation of lesion clustering in irradiated plasmid DNA. Int J Radiat Biol 2005;81:41–54.

http://dx.doi.org/10.1080/09553000400017895.

[63] Ludek V, Pachnerova Brabcova K, Stepan V, Moretto-Capelle P, Bugler B, Legube G, et al. Proton-induced direct and indirect damage of plasmid DNA. Radiat Environ Biophys 2015;54:343–52. http://dx.doi.org/10.1007/s00411-015-0605-6.

[64] Souici M, Khalil TT, Muller D, Raffy Q, Barillon R, Belafrites A, et al. Single- and double-strand breaks of dry DNA exposed to protons at Bragg-peak energies. J Phys Chem B 2017;121:497–507. http://dx.doi.org/10.1021/acs.jpcb.6b11060.